

# Distribution Agnostic Symbolic Representations for Time Series Dimensionality Reduction and Online Anomaly Detection

Konstantinos Bountrogiannis, George Tzagkarakis, Panagiotis Tsakalides, *Member, IEEE*

**Abstract**—Due to the importance of the lower bounding distances and the attractiveness of symbolic representations, the family of symbolic aggregate approximations (SAX) has been used extensively for encoding time series data. However, typical SAX-based methods rely on two restrictive assumptions; the Gaussian distribution and equiprobable symbols. This paper proposes two novel data-driven SAX-based symbolic representations, distinguished by their discretization steps. The first representation, oriented for general data compaction and indexing scenarios, is based on the combination of kernel density estimation and Lloyd-Max quantization to minimize the information loss and mean squared error in the discretization step. The second method, oriented for high-level mining tasks, employs the Mean-Shift clustering method and is shown to enhance anomaly detection in the lower-dimensional space. Besides, we verify on a theoretical basis a previously observed phenomenon of the intrinsic process that results in a lower than the expected variance of the intermediate piecewise aggregate approximation. This phenomenon causes an additional information loss but can be avoided with a simple modification. The proposed representations possess all the attractive properties of the conventional SAX method. Furthermore, experimental evaluation on real-world datasets demonstrates their superiority compared to the traditional SAX and an alternative data-driven SAX variant.

**Index Terms**—Time series analysis, symbolic representations, kernel methods, dynamic clustering, anomaly detection, streaming data

## 1 INTRODUCTION

DATA representation in a lower-dimensional space is a central topic in storing and mining the ever increasing amount of time series becoming available thanks to the advances in computing and sensing technologies. Certainly, the extraction of descriptive motifs of reduced dimensionality, which provide a meaningful, yet compact, representation of the original inherent information, has been an ongoing research field for the last few decades.

At the core of time series representations is the definition of appropriate distance measures in the lower-dimensional space. More precisely, the transformation of data objects to a lower-dimensional subspace should be, ideally, distance-preserving. This property would allow data mining tasks to perform equally well in the lower-dimensional space as in the higher-dimensional one. However, except for trivial cases, distance measures defined in lower-dimensional spaces can only approximately preserve distances.

*This work is funded by the Hellenic Foundation for Research and Innovation (HFRDI) and the General Secretariat for Research and Technology (GSRT) under grant agreements No. 2285 (neuronXnet) and No. 1725 (V4-ICARUS).*

- K. Bountrogiannis and P. Tsakalides are with the Computer Science Department, University of Crete, Crete, Greece and with the Institute of Computer Science, Foundation for Research and Technology-Hellas, Crete, Greece.  
E-mail: {kbountrogiannis, tsakalid}@csd.uoc.gr
- G. Tzagkarakis is with the Institute of Computer Science, Foundation for Research and Technology-Hellas, Crete, Greece.  
E-mail: gtzag@ics.forth.gr

© 2021 IEEE. Personal use of this material is permitted. Permission from IEEE must be obtained for all other uses, in any current or future media, including reprinting/republishing this material for advertising or promotional purposes, creating new collective works, for resale or redistribution to servers or lists, or reuse of any copyrighted component of this work in other works.

A milestone for the definition and utilization of such measures has been the discovery of the properties of lower-bounding distances [1]. That is, when the distance measure in the lower-dimensional space lower-bounds the distance of the same objects in the higher-dimensional space, it is proved that approximate queries in the lower-dimensional space (i.e., queries that return all objects with up to a maximum distance from the query object), return no false dismissals. In advance, the tighter this bound is, the less false alarms are returned.

The symbolic aggregate approximation (SAX) introduced in [2] is the first symbolic representation to possess the lower-bounding property. Symbolic representations have the advantage of exploiting the wealth of search algorithms used in bioinformatics and text mining communities, in conjunction to enabling the exploitation of numerous data mining techniques that require discrete data. On top of that, SAX is characterized by conceptual simplicity and computational tractability. These properties have rendered SAX arguably the most widely used time series representation for monitoring, processing and mining data from numerous sources and in distinct application domains, including physiological data [3], space telemetry [4], computational biology [5], smart grids [6], building systems [7], and stock market [8], just to name a few.

In this paper, we propose two efficient alternative discretization schemes resulting in a couple of novel SAX representations. The proposed methods are non-parametric and data-driven, and are shown to effectively exploit the underlying distribution of the data towards increasing the accuracy of the representations. Both methods rely on kernel-

based techniques to estimate the underlying data statistics.

The first method, hereafter referred to as probabilistic SAX (pSAX), is based on a kernel density estimator (KDE) [9] to estimate the density function of the data source, coupled with a Lloyd-Max quantizer [10], [11] for computing optimal discretization intervals. This representation is tailored to general data compaction and indexing scenarios. The second method, hereafter referred to as clustering SAX (cSAX), relies on the mean-shift clustering method [12], [13] to produce descriptive symbolic sequences, which are more appropriate for high-level data analysis tasks. The performance of the latter method is evaluated on the task of anomaly detection. Both methods preserve the lower-bounding property, whilst pSAX exhibits tighter lower bounds than the conventional SAX. Furthermore, both methods are experimentally compared against the conventional SAX and an alternative data-driven method, the so-called aSAX [14], which employs the  $k$ -means algorithm for the discretization step.

The contribution of this paper also comprises: i) a thorough information-theoretic analysis of the SAX technique, in terms of information loss; ii) a theoretical verification, along with a practical solution, of a previously observed phenomenon, where the data variance after the intermediate step of piecewise aggregate approximation is lower than the expected [15]; iii) a dynamic clustering criterion for the mean-shift method; and iv) the definition of two novel distance measures, which are not lower-bounding, but are optimal in the sense of mean squared error. The latter is of importance in data mining applications, where there is no need to identify the time series within a strict distance of the query. In those cases, the lower-bounding property is irrelevant and a minimum-error distance measure is more effective [16].

The rest of this paper is organized as follows. Section 2 overviews the SAX technique, along with the anomaly detection method that is utilized for testing cSAX. Section 3 quantifies the information loss of SAX and provides guidelines for its minimization. Section 4 analyzes the key components employed by our proposed symbolic representations, whilst Sections 5 and 6 provide the implementation details of pSAX and cSAX, respectively. Section 7 evaluates the performance of our proposed methods on a set of distinct time series data. Finally, Section 8 summarizes the main outcomes and gives directions for further work.

## 2 PRELIMINARIES

### 2.1 Symbolic Aggregate Approximation

This section overviews briefly the main concepts of the conventional SAX method [2]. The core of SAX consists of a two-step transformation that reduces the dimensionality of the data, coupled with the definition of an appropriate distance measure in the lower-dimensional space that lower bounds the Euclidean distance in the original space.

Let  $\mathcal{T}^N = \{X : X = (x_1, x_2, \dots, x_N)\}$  denote the set of all  $N$ -length continuous (real-valued) time series objects and  $\mathcal{C}_A^N = \{C : C = (c_1, c_2, \dots, c_N), c_i \in A\}$  the set of all  $N$ -length discrete time series objects with values from an alphabet  $A$  of size  $|A| = \kappa$ . Given a time series  $X \in \mathcal{T}^N$ , a

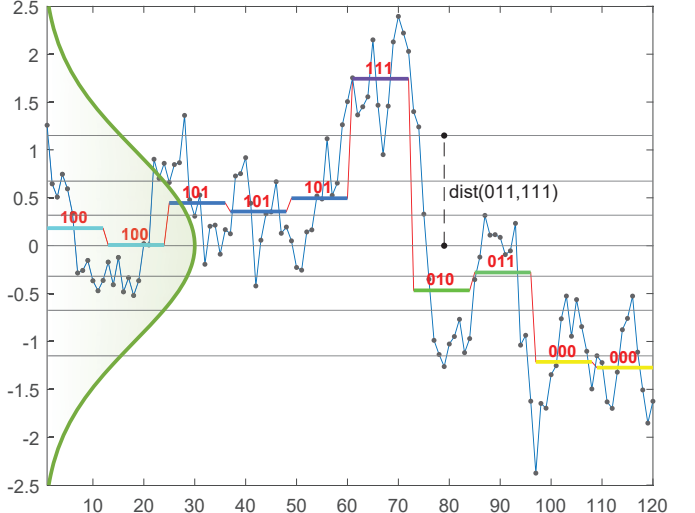


Fig. 1. SAX representation of a time series. In this example, a time series of length  $N = 120$  is first transformed into its PAA representation by segmenting and averaging the series into  $M = 12$  pieces. Then, each segment is assigned a binary codeword, subject to which of the  $\kappa = 8$  equiprobable intervals of the standard Gaussian pdf it falls in. Each quantization interval is bounded by two cutlines and is assigned a codeword from the alphabet  $A = \{0_2, 1_2, \dots, 7_2\}$ .

Z-normalization is performed as a preprocessing step prior to the application of a SAX transformation,

$$X' = \frac{X - \mu_X}{\sigma_X}, \quad (1)$$

where  $\mu_X$  and  $\sigma_X$  are the mean and standard deviation of  $X$ , respectively. For convenience, hereafter  $X$  is assumed to be Z-normalized à priori.

The first step of SAX consists of a piecewise aggregate approximation (PAA)  $\mathcal{T}^N \rightarrow \mathcal{T}^M$ , which transforms a given time series  $X \in \mathcal{T}^N$  into another time series  $Y = (y_1, \dots, y_M) \in \mathcal{T}^M$  with reduced dimensionality  $M < N$ . For this,  $X$  is divided into  $M$  equal-sized segments and the average value is calculated for each segment. The second step performs a discretization  $\mathcal{T}^M \rightarrow \mathcal{C}_A^M$  that maps  $y_i \in \mathbb{R}$  to  $c_i \in A$ . The discretization scheme adopted by SAX employs an equiprobable quantization of  $y_i$ ,  $i = 1, \dots, M$ , under the assumption that  $y_i \sim \mathcal{N}(0, 1)$ . Under this assumption,  $y_i$ 's are quantized within  $\kappa$  equiprobable intervals under the Gaussian probability density curve. The two-step transformation  $\mathcal{T}^N \rightarrow \mathcal{T}^M \rightarrow \mathcal{C}_A^M$  results in a SAX representation of length  $M$  for the alphabet  $A$ . The ratio  $M/N$  determines the degree of dimensionality reduction. Fig. 1 illustrates the two-step process of SAX.

It is known that, in order to guarantee the absence of false dismissals when performing a similarity search in the lower-dimensional space, it suffices to define a distance measure in the lower-dimensional space that lower bounds the distance in the original space (ref. [1]). Let  $C, Q \in \mathcal{C}_A^M$  be the SAX representations of two time series  $U \in \mathcal{T}^N$  and  $S \in \mathcal{T}^N$ , respectively. Then, a lower-bounding distance measure is defined as follows,

$$\text{mindist}(C, Q) = \sqrt{\frac{N}{M} \sum_{i=1}^M (\text{dist}(c_i, q_i))^2}, \quad (2)$$

where  $dist(c_i, q_i)$  is the absolute difference of the two closest cutlines that respectively bound the intervals of  $c_i$  and  $q_i$  (ref. Fig. 1 for an example). Furthermore, if  $Y \in \mathcal{T}^M$  is the PAA of  $U$  and  $Q \in \mathcal{C}_A^M$  is the SAX representation of  $S$ , a tighter lower bounding distance measure is defined by

$$mindist\_PAA(Y, Q) = \sqrt{\frac{N}{M} \sum_{i=1}^M \begin{cases} (\beta_{L_i} - y_i)^2, & \beta_{L_i} > y_i \\ (\beta_{U_i} - y_i)^2, & \beta_{U_i} < y_i \\ 0, & \text{otherwise} \end{cases}}, \quad (3)$$

where  $\beta_{L_i}$  and  $\beta_{U_i}$  are the lower and upper cutlines of the codeword  $q_i$ .

The tightness of lower bound (TLB) is the degree of closeness of the  $mindist\_PAA(Y, Q)$  to the true distance of the data. The higher it is, the lower the rate of false positives in a similarity search. The TLB is defined as follows,

$$TLB(U, S) = \frac{mindist\_PAA(Y, Q)}{d(U, S)}, \quad (4)$$

where  $d(U, S)$  is the distance in the original time series space.

Because the discretization step  $\mathcal{T}^M \rightarrow \mathcal{C}_A^M$  quantizes the PAA samples into  $\kappa$  equiprobable intervals, when the Gaussian assumption is valid, the generated symbolic sequence is uniformly distributed.

Although not stated clearly in the introductory paper [2], the selection of equiprobable intervals is typically based on the fact that the uniform distribution maximizes the entropy of the symbolic sequence. This implies that a pair of time-series is more easily distinguishable in the lower-dimensional space.

An advantage of our proposed method is that the discretization step is optimized for general data mining applications, such that the mean squared error (MSE) is minimized. Moreover, we demonstrate that MSE minimization yields an improved performance when compared against entropy maximization, in terms of TLB (4).

## 2.2 Anomaly Detection via Statistical Hypothesis Testing

A non-parametric method for online anomaly detection has been proposed in [17]. The method proceeds in a rolling window fashion, employing a goodness-of-fit criterion to test whether the most recent window of  $n$  samples is distributed similarly with the past samples. In particular, the null hypothesis of the test is a composite hypothesis consisting of the union of empirical distributions for a collection of past  $n$ -length windows. Then, the null hypothesis is partitioned into multiple simple hypotheses, which are tested separately. In practice, a similarity test is performed between the current window and each previous window independently. A similarity condition is assumed to be satisfied if the current window fits with the distribution of at least one of the previous windows. If the null hypothesis is rejected, the current window is flagged as anomalous, whilst if the null hypothesis is accepted, the current window is flagged as normal. The above process is summarized in Algorithm 1.

An interesting observation regarding Algorithm 1 is that the earliest windows will always be considered as anomalous, as there will be very few pieces in the null hypothesis

to test against. At this stage, the method learns the most diverse representations of the data and saves them as part of the null hypothesis. Gradually, the null hypothesis makes a good representation of the data and acts as a ground truth model to test the goodness of fit for future windows.

### Algorithm 1: Anomaly Detection via Goodness of Fit

**Input:**  $x$  (time series),  $n$  (window length),  $\alpha$  (significance level)

```

1:  $\rho_{thr} = F_{T,n}^{-1}(1 - \alpha)$ 
2:  $c \leftarrow 0$  \\\ nul hypothesis count
3:  $i \leftarrow n$  \\\ sample index
4: while new data arrives do
5:   if  $T(x[i-n+1:i], H_{0j}) < \rho_{thr}$ , for any null
     hypothesis component  $H_{0j}$ ,  $j \leq c$  then
6:     Declare window as non-anomalous
7:   else
8:     Declare window as anomalous
9:    $c \leftarrow c + 1$ 
10:   $H_{0c} \leftarrow x[i-n+1:i]$ 
11: end if
12:  $i \leftarrow i + 1$ 
13: end while

```

Furthermore, as stated in [17], the specific test statistic,  $T$ , employed by Algorithm 1 is defined by:

$$T(X, Q) \triangleq 2 \cdot n \cdot D_{KL}(P_X \parallel P_Q), \quad (5)$$

where  $P_X$  and  $P_Q$  are the empirical mass functions of  $X$  and  $Q$ , respectively, and  $D_{KL}(P_X \parallel P_Q)$  is the Kullback-Leibler divergence between the mass functions  $P_X$  and  $P_Q$ :

$$D_{KL}(P_X \parallel P_Q) \triangleq \sum_{x \in \mathcal{X}} P_X(x) \log \frac{P_X(x)}{P_Q(x)}, \quad (6)$$

with the convention that  $0 \log 0 = 0$ .

It is known that  $T(X, Q)$  converges in distribution to a random variable that follows the  $\chi^2$  distribution with  $\kappa - 1$  degrees of freedom, where  $\kappa$  is the cardinality of the sample space. In light of this observation, the threshold in line 1 is computed by the inverse cumulative distribution function of the  $\chi^2$  distribution with  $\kappa - 1$  degrees of freedom. The significance level  $\alpha$  specifies the sensitivity of the test.

## 3 STATISTICAL AND INFORMATION-THEORETIC ISSUES OF SAX

### 3.1 The Gaussian Assumption

Although the Gaussian model is commonly used to describe the statistics in a broad range of data sources due to its theoretical justification and computational tractability, the normality assumption is often violated in various practical applications. As such, a mismatch in the distribution yields an information loss that can be quantified by the Kullback-Leibler divergence. As we analyze in Sec. 7.1, this information loss degrades the performance of SAX.

In the following, we quantify the information that is lost during data source quantization due to a mismatch between the Gaussian distribution assumption and the actual underlying data distribution. The amount of lost information is described by the increment in the average number of

bits required to describe a sample with a specific precision, when the assumed distribution is wrong. To do so, first we introduce the differential entropy and the Kullback-Leibler divergence of continuous random variables.

The differential entropy  $h(f_X)$  of a continuous random variable  $X$  with pdf  $f_X(x)$  is defined by

$$h(f_X) \triangleq - \int f_X(x) \log f_X(x) dx, \quad (7)$$

where the integration is performed in the regions of the sample space where  $f_X(x) > 0$ . Entropy is measured in *bits* if the log base is 2 and in *nats* if it is  $e$ .

The Kullback-Leibler divergence  $D_{KL}(f_X \parallel f_G)$  between the probability densities  $f_X(x)$ ,  $f_G(x)$  (in this order) is defined by

$$D_{KL}(f_X \parallel f_G) \triangleq \int f_X(x) \log \frac{f_X(x)}{f_G(x)} dx, \quad (8)$$

with the convention that  $0 \log 0 = 0$ . Notice that

$$D_{KL}(f_X \parallel f_G) \geq 0, \quad (9)$$

with equality iff  $f_X(x) = f_G(x)$  almost everywhere. Furthermore,

$$D_{KL}(f_X \parallel f_G) = h(f_X, f_G) - h(f_X), \quad (10)$$

where  $h(f_X, f_G) \triangleq \int f_X(x) \log f_G(x) dx$  is the continuous cross-entropy.

Let  $X^\Delta$  denote the quantized version of  $X$ , defined by

$$X^\Delta = x_i, \text{ if } i\Delta \leq X < (i+1)\Delta. \quad (11)$$

Then, the probability mass function (pmf) of  $X^\Delta$  is given by [18, Sec. 8.3]:

$$P(x_i) = \int_{i\Delta}^{(i+1)\Delta} f_X(x) dx. \quad (12)$$

For convenience in calculations, the above expressions rely on quantization intervals of equal length  $\Delta$ . However, for any quantization scheme it holds that, as the number of the quantization intervals approaches infinity, they become equally infinitesimal.

The next theorem provides upper and lower bounds for the expected description length of  $X^\Delta$  and is the continuous analog of [18, Thm. 5.4.3].

**Theorem 3.1.** *The expected description length,  $\mathbb{E}[l(X^\Delta)]$ , of the random variable  $X^\Delta$ , assuming optimal coding under the probability density function  $f_G(x)$ , is bounded as follows,*

$$\begin{aligned} \mathbb{E}[l(X^\Delta)] &\geq h(f_X) + D_{KL}(f_X \parallel f_G) + \log \frac{1}{\Delta}, \\ \mathbb{E}[l(X^\Delta)] &< h(f_X) + D_{KL}(f_X \parallel f_G) + \log \frac{1}{\Delta} + 1. \end{aligned} \quad (13)$$

The detailed proof is derived in the Appendix. Notice that the additive term  $\log \frac{1}{\Delta}$  is the contribution of the quantization. Theorem 3.1 together with (9) denote that the information loss by assuming that the distribution of  $X$  is equal to  $f_G(x)$  instead of  $f_X(x)$  is given by  $D_{KL}(f_X \parallel f_G)$ . This is similar to the result derived in the case of discrete random variables. When  $f_G(x)$  is the Gaussian density function, the following corollary holds.

**Corollary.** *Let  $X$  be an arbitrary continuous random variable with density  $f_X(x)$ , with mean  $\mu_X$  and variance  $\sigma_X^2$ , and  $G$  a Gaussian random variable,  $G \sim \mathcal{N}(\mu_G, \sigma_G^2)$ , whose density is denoted by  $f_G(x)$ . Then,*

$$D_{KL}(f_X \parallel f_G) = \ln \sigma_G \sqrt{2\pi} + \frac{1}{2\sigma_G^2} \int f_X(x)(x - \mu_G)^2 dx - h(f_X), \quad (14)$$

measured in *nats*.

*Proof.*

$$\begin{aligned} h(f_X, f_G) &= - \int f_X(x) \ln f_G(x) dx \\ &= - \int f(x) \ln \frac{1}{\sqrt{2\pi\sigma_G^2}} e^{-(x-\mu_G)^2/(2\sigma_G^2)} dx \\ &= - \int f_X(x) \left( \ln \frac{1}{\sqrt{2\pi\sigma_G^2}} - \frac{(x-\mu_G)^2}{2\sigma_G^2} \right) dx \\ &= - \int f_X(x) \ln \frac{1}{\sqrt{2\pi\sigma_G^2}} dx + \int f_X(x) \frac{(x-\mu_G)^2}{2\sigma_G^2} dx \\ &= \ln \sigma_G \sqrt{2\pi} + \frac{1}{2\sigma_G^2} \int f_X(x)(x - \mu_G)^2 dx. \end{aligned} \quad (15)$$

Combining (10) and (15) completes the proof.  $\square$

Under the constraints that  $\mu_X = \mu_G = 0$  and  $\sigma_X = \sigma_G = 1$ , which is the case in SAX due to Z-normalization, (14) reduces to

$$\begin{aligned} D_{KL}(f_X \parallel f_G) &= \ln \sqrt{2\pi} + \frac{1}{2} \int f_X(x)x^2 dx - h(f_X) \\ &= \ln \sqrt{2\pi} + \frac{1}{2} \cdot 1 - h(f_X) \\ &= \ln \sqrt{2\pi e} - h(f_X) \quad \text{nats} \\ &= \frac{1}{\ln 2} (\ln \sqrt{2\pi e} - h(f_X)) \quad \text{bits}. \end{aligned} \quad (16)$$

Eq. (16) quantifies the information loss in the discretization step of SAX.

### 3.2 Z-normalization and Piecewise Aggregate Approximation

This section elaborates on a fundamental misunderstanding when applying the conventional SAX method. Specifically, even when the Gaussian assumption holds for a given data set, performing a Z-normalization on the input data does not guarantee a standard distribution for the PAA sequence.

To verify this statement, consider the case where a time series  $X \in \mathcal{T}^N$  is a sequence of correlated and jointly Gaussian-distributed random variables. We set  $M = N/m$ , that is, the PAA transformation  $X \rightarrow Y$  is given by  $y_i = [\sum_{k=m(i-1)+1}^{mi} x_k]/m$ ,  $i = 1, \dots, M$ . We assume that the samples are Z-normalized, thus  $x_k \sim \mathcal{N}(0, 1) \forall k = 1, \dots, N$  and we denote by  $\bar{\rho}$  the average pairwise Pearson's correlation of the distinct sample pairs. Then, it can be derived in a straightforward manner that  $y_i \sim \mathcal{N}(\mu_Y, \sigma_Y^2)$ , where

$$\mu_Y = 0, \quad \sigma_Y^2 = \frac{1 + (m-1)\bar{\rho}}{m}. \quad (17)$$

That is, the PAA sequence  $Y$  follows a standard Gaussian distribution only when  $\bar{\rho} = 1$ .

The above theoretical proof explains the experimental results described in [15], where the authors observe that the PAA step reduces the resulting standard deviation.

Notice that in Sec. 3.1 the PAA sequence was assumed to have a unit variance. Nevertheless, if Z-normalization is performed prior to the PAA step, then,  $\sigma_Y^2 \leq 1$  as showed above, where the strict inequality holds for  $\bar{\rho} < 1$ . In this case, the information loss (14) in the discretization step is equal to

$$D_{KL}(f_Y \parallel f_G) = \frac{1}{\ln 2} \left( \ln \sqrt{2\pi} + \frac{1}{2} \sigma_Y^2 - h(f_Y) \right) \text{ bits,} \quad (18)$$

where  $f_Y(y)$  is the pdf of  $Y$ . By noticing that the effect of the standard deviation on the differential entropy is an additive  $\log$  term, the right side of (18) is larger than the one of (16) by  $((\sigma_Y^2 - 1)/2 - \ln \sigma_Y) / \ln 2$ .

Based on the above derivations and remarks, it becomes clear that there exists an inherent mistake in the default SAX procedure that induces an additional information loss. This is due to the fact that the PAA sequence is assumed to have unit standard deviation, which is not true.

To address this issue, we propose a simple, yet effective, solution. Specifically, instead of performing a Z-normalization on the original data samples, the PAA samples are Z-normalized directly which also guarantees their unit variance.

## 4 DATA-DRIVEN SAX-BASED SYMBOLIC REPRESENTATIONS

Motivated by the remarks in the previous section, we introduce a new family of SAX-based symbolic representations. The proposed representations adapt directly to the inherent data statistics, minimizing the information loss (16) in the discretization step. In addition, we enable increased flexibility in utilizing appropriate quantization schemes depending on the desired application scenario. In particular, our representations rely on the efficacy of kernel density estimators (KDE) [9] for modelling the probability distribution of the data. The estimated density function is then employed by a density-based discretization method to provide an accurate representation of the PAA sequence. In the following, the main concepts of KDE are briefly overviewed, along with the discretization methods that are at the core of our data-driven SAX representations.

### 4.1 Kernel Density Estimation

Kernel density estimation [9] is a method for estimating the probability density function of a data source. Essentially, it is the summation of a set of translated and dilated kernel functions centered at each observed sample,

$$\hat{f}_{h,K}(x) = \frac{1}{Nh} \sum_{i=1}^N K\left(\frac{x - x_i}{h}\right), \quad (19)$$

where  $x_i, i = 1, \dots, N$ , are the observed samples,  $K(\cdot)$  is the kernel function that controls the weight given to the neighboring samples of  $x \in X$ , and  $h$  is a smoothness parameter, which controls the width of the kernel. In general, the smoothness parameter  $h$  affects more the accuracy of the estimator than the kernel function itself.

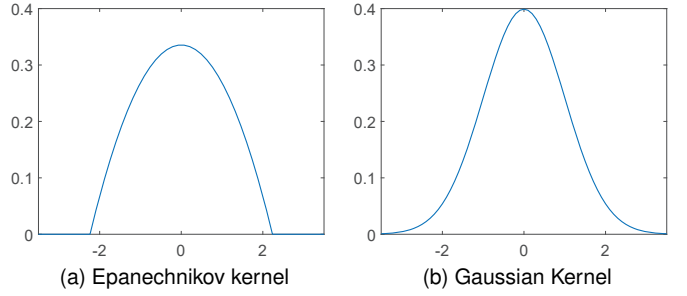


Fig. 2. The kernel functions employed by our proposed method for density estimation.

Under suitable conditions, the optimal kernel, in terms of the asymptotic minimum integrated squared error (AMISE) between the estimated and the target density function, is proved to be the Epanechnikov kernel [19], shown in Fig. 2a. Another commonly used kernel is the Gaussian kernel, shown in Fig. 2b. These two kernels are defined by:

$$\text{Epanechnikov: } K(x) = \max\left(0, \frac{3}{4\sqrt{5}}\left(1 - \frac{x^2}{5}\right)\right) \quad (20)$$

$$\text{Gaussian: } K(x) = \frac{1}{\sqrt{2\pi}} e^{-\frac{1}{2}x^2} \quad (21)$$

For a given kernel function, the optimal value for  $h$ , in terms of a minimum AMISE, is given by

$$h_{opt} = \left[ \frac{\int_{-\infty}^{+\infty} K^2(y) dy}{N\mu_2^2 \int_{-\infty}^{+\infty} (f''(x))^2 dx} \right]^{1/5}, \quad (22)$$

where  $K(x)$  is the chosen kernel function,  $\mu_2$  is the second moment of  $K(x)$ , and  $f(x)$  is the target pdf.

Since in practice the knowledge of the true target pdf is typically not available, the authors in [20] suggested that a known family of distributions can be used to calculate  $f''(x)$ . The Gaussian is the most commonly used distribution, which yields the following approximation for the optimal smoothness parameter,

$$h_{opt}^N = \hat{\sigma} \cdot \left[ \frac{8\sqrt{\pi} \int_{-\infty}^{+\infty} K^2(y) dy}{3N\mu_2^2} \right]^{1/5}, \quad (23)$$

where  $\hat{\sigma}$  is the estimated standard deviation of the data.

For the Epanechnikov and Gaussian kernels, the following values are replaced in (23),

$$\text{Epanechnikov: } \int_{-\infty}^{+\infty} K^2(y) dy = \frac{3}{5}, \quad \mu_2 = \frac{1}{5} \quad (24)$$

$$\text{Gaussian: } \int_{-\infty}^{+\infty} K^2(y) dy = \frac{1}{2\sqrt{\pi}}, \quad \mu_2 = 1 \quad (25)$$

yielding the following optimal smoothness parameters,

$$\text{Epanechnikov: } h_{opt}^N = 2.3449 \cdot \hat{\sigma} \cdot N^{-1/5} \quad (26)$$

$$\text{Gaussian: } h_{opt}^N = 1.0492 \cdot \hat{\sigma} \cdot N^{-1/5} \quad (27)$$

The expressions in (26), (27) are referred as Silverman's rules of thumb.

If some wishes to estimate the derivative of a density function, rather than the function itself, then the AMISE

analysis yields different optimal parameters. Particularly, similar calculations as before give the following results:

$$\text{Epanechnikov kernel: } h_{\nabla, \text{opt}}^N = 1.5232 \cdot \hat{\sigma} \cdot N^{-1/7} \quad (28)$$

$$\text{Gaussian kernel: } h_{\nabla, \text{opt}}^N = 0.9686 \cdot \hat{\sigma} \cdot N^{-1/7} \quad (29)$$

The latter result shall be useful for estimating the modes of the density. In the proposed framework, we employ both the Epanechnikov and the Gaussian kernel, with the choice of the kernel function depending on the specific discretization scheme that follows.

## 4.2 Discretization Schemes

Two distinct methods are employed in the discretization step, namely, (i) the Lloyd-Max quantizer and (ii) the mean-shift clustering algorithm. A visual comparison of the different data-driven discretization schemes is depicted in Figs. 3a-3c.

### 4.2.1 Lloyd-Max Quantization

The Lloyd-Max quantizer [10], [11] is an alternating MSE minimization algorithm. Let  $\{X_1, \dots, X_\kappa\}$  be a partition of the sample space  $\mathcal{X}$ , where  $X_i$ 's are disjoint subsets with an arbitrary number of input elements from  $\mathcal{X}$ , and  $\{c_1, \dots, c_\kappa\}$  be a set of codewords. Then, the quantization mapping  $Q(\cdot)$  is defined by

$$Q(x_j) = c_i, \quad \forall x_j \in X_i. \quad (30)$$

The number of quantization intervals,  $\kappa$ , is a predefined parameter of the quantization process.

Let  $d(x - Q(x))$  denote a distance measure between an input element and the codeword assigned to it. If  $f(x)$  is the underlying probability density function of the input space, and  $b_i, b_{i+1}$  are the infimum and supremum of the subset  $X_i$ , respectively, then, the distortion  $D$  is defined as the expected value of  $d$ , that is,

$$D = \mathbb{E}_f[d(x - Q(x))] = \sum_{i=1}^{\kappa} \int_{b_i}^{b_{i+1}} d(x - c_i) f(x) dx. \quad (31)$$

The necessary criteria for minimizing the distortion function  $D$  are derived by calculating the partial derivatives with respect to  $b_i$ 's and  $c_i$ 's and setting them equal to zero. In the special case where the distance measure  $d$  is the Euclidean distance, the computations yield the following necessary criteria:

$$b_i = (c_i + c_{i-1})/2, \quad i = 2, \dots, \kappa \quad (32)$$

$$c_i = \frac{\int_{b_i}^{b_{i+1}} x f(x) dx}{\int_{b_i}^{b_{i+1}} f(x) dx}, \quad i = 1, \dots, \kappa \quad (33)$$

That is,  $b_i$  must be equal to the midpoint of  $c_i$  and  $c_{i-1}$ , whilst  $c_i$  must be the centroid of subset  $X_i$ . Note that the above criteria are necessary but not sufficient. In order to be sufficient, the Hessian matrix of the distortion function must be positive definite.

Due to their mutual relationship, the solution of (32) and (33) is approximated iteratively by alternating between the necessary criteria. The process is summarized in Algorithm 2, while a visual example is illustrated in Fig. 3b.

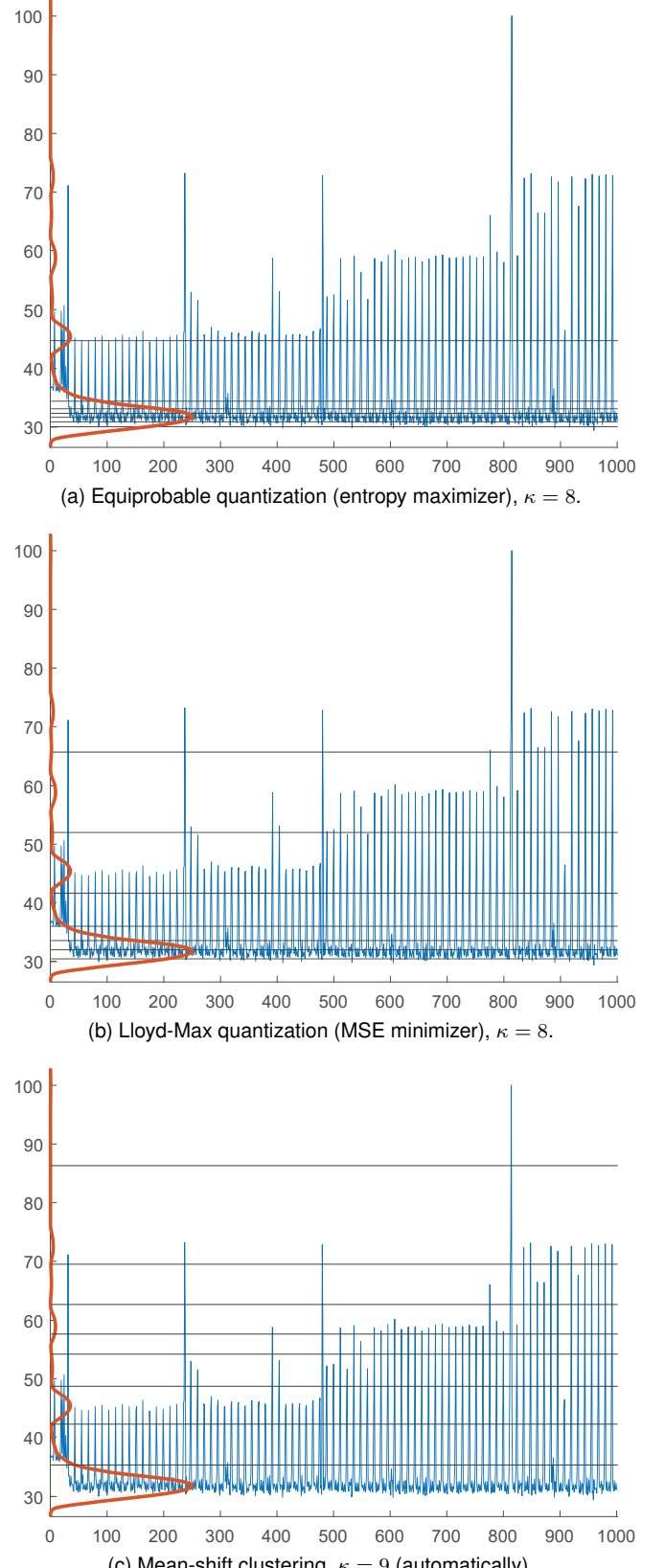


Fig. 3. Various density-based discretization schemes. The density is estimated via KDE. Conventional SAX employs equiprobable quantization, but assuming Gaussian distribution (ref. Fig. 1). Our pSAX employs the Lloyd-Max quantizer and csAX employs the mean-shift clustering. Notice the decreasing amount of energy in the dominant mode.

**Algorithm 2:** Lloyd-Max Quantizer

**Input:**  $f(x)$  (probability density function)

- 1: Initialize range:  $b_1 \leftarrow -\infty, b_{\kappa+1} \leftarrow +\infty$ .
- 2: Initialize codewords randomly  $c_i \in (b_1, b_{\kappa+1}), i = 1, \dots, \kappa$ .
- 3: **repeat**
- 4:    $b_i \leftarrow (c_i + c_{i-1})/2, \text{ for } i = 2, \dots, \kappa$
- 5:    $c_i \leftarrow \frac{\int_{b_i}^{b_{i+1}} xf(x)dx}{\int_{b_i}^{b_{i+1}} f(x)dx}, \text{ for } i = 1, \dots, \kappa$
- 6: **until** convergence

#### 4.2.2 Mean-Shift Clustering

Mean-shift clustering [12], [13] is based on the rationale that the generated samples form clusters corresponding to regions with high local probability density. That is, the clusters correspond to the modes of the underlying probability density function. In the following, we describe the procedure for uni-dimensional signals, however, the generalization to higher-dimensional signals follows in a straightforward way.

Given the outcome of the KDE process (19), the modes of the estimated density function  $\hat{f}_{h,K}(x)$  are found next. The mean-shift approach estimates the modes by relying on kernels that are symmetric around zero and can be expressed as

$$K(x) = z_k k(\|x\|^2), \quad (34)$$

where  $z_k$  is a normalization constant parameter that enforces  $K(x)$  to integrate to one. The function  $k(x)$  is called the *profile* of  $K(x)$ .

By employing (34), the estimator in (19) is given by

$$\hat{f}_{h,K}(x) = \frac{z_k}{Nh} \sum_{i=1}^N k\left(\left\|\frac{x - x_i}{h}\right\|^2\right). \quad (35)$$

Then, the modes are found by detecting the points where the gradient  $\nabla \hat{f}_{h,K}(x)$  equals zero. These points are the stationary points, including all the local maxima, that is, the modes of the density function  $\hat{f}_{h,K}(x)$ . The gradient is given by

$$\nabla \hat{f}_{h,K}(x) = \frac{2z_k}{Nh^3} \sum_{i=1}^N (x - x_i) k'\left(\left\|\frac{x - x_i}{h}\right\|^2\right). \quad (36)$$

Defining the profile  $g(x) = -k'(x)$  and the corresponding kernel  $G(x) = z_g g(\|x\|^2)$ , the gradient (36) equals

$$\begin{aligned} \nabla \hat{f}_{h,K}(x) &= \frac{2z_g}{Nh^3} \sum_{i=1}^N (x - x_i) g\left(\left\|\frac{x_i - x}{h}\right\|^2\right) \\ &= \frac{2z_g}{Nh^3} \left[ \sum_{i=1}^N x_i g\left(\left\|\frac{x_i - x}{h}\right\|^2\right) - x \sum_{i=1}^N g\left(\left\|\frac{x_i - x}{h}\right\|^2\right) \right] \\ &= \frac{2z_g}{Nh^3} \left[ \sum_{i=1}^N g\left(\left\|\frac{x_i - x}{h}\right\|^2\right) \right] \left[ \frac{\sum_{i=1}^N x_i g\left(\left\|\frac{x_i - x}{h}\right\|^2\right)}{\sum_{i=1}^N g\left(\left\|\frac{x_i - x}{h}\right\|^2\right)} - x \right] \end{aligned} \quad (37)$$

The second term of the last equation in (37) is called the *mean-shift* vector  $m_{h,g}$ ,

$$m_{h,g} \triangleq \frac{\sum_{i=1}^N x_i g\left(\left\|\frac{x_i - x}{h}\right\|^2\right)}{\sum_{i=1}^N g\left(\left\|\frac{x_i - x}{h}\right\|^2\right)} - x, \quad (38)$$

which can be rewritten in terms of the estimated density function as follows,

$$m_{h,g} = \frac{Nh^2}{2z_k} \cdot \frac{\nabla \hat{f}_{h,K}(x)}{\hat{f}_{h,G}(x)}. \quad (39)$$

The above equation implies that the mean-shift vector points at the same direction as the gradient of the estimated density  $\hat{f}_{h,K}(x)$ , which is the direction with the highest increase in density. Furthermore, it is inversely proportional to  $\hat{f}_{h,G}(x)$ , which affects the mean-shift vector by decreasing its value in the areas with high density, that is, near the modes of the density function. These remarks lead to the formulation of the mean-shift procedure, which is essentially a gradient ascend algorithm with a self-adjusted step-size. The mean-shift clustering algorithm is summarized in Algorithm 3, while a visual example is illustrated in Fig. 3c.

**Algorithm 3:** Mean-Shift Clustering

- 1: **while** stopping criteria are not met **do**
- 2:   Pick a random sample  $x$ .
- 3:   **repeat**
- 4:     Compute the mean-shift  $m_{h,g}(x)$ .
- 5:     Move to the next sample in the direction and step-size of  $m_{h,g}(x)$ .
- 6:   **until** convergence
- 7: **end while**

In the mean-shift nomenclature,  $K(x)$  is called the *shadow* of  $G(x)$ . The Gaussian kernel is the only kernel that is the shadow of itself.

## 5 DATA-DRIVEN SAX WITH TIGHT LOWER BOUNDING DISTANCES

This section analyzes our proposed data-driven symbolic representation, hereafter called probabilistic SAX (pSAX), which achieves tighter lower-bounding distances than the previous SAX-based counterparts. Furthermore, our method performs in a completely distribution agnostic framework, without any prior assumption for the data distribution. As such, it is an improved alternative to the conventional SAX representations for general data mining and indexing scenarios, where the data generating process is often unknown and the tightness of lower bound (TLB) (cf. (4)) is of utmost importance.

To this end, our method applies a kernel density estimator (KDE) (ref. Sec. 4.1) directly after the PAA step, in order to estimate the underlying probability density function of the PAA sequence, without any prior probabilistic assumption. Subsequently, the KDE step is coupled with a Lloyd-Max quantizer, as described in Sec. 4.2.1, to estimate the optimal quantization intervals.

Notice also that, since our method does not rely on any prior assumption on the distribution of either the data or PAA, the  $Z$ -normalization step is needless. Nevertheless, in light of the observations made in Sec. 3.2, we estimate the density function of the PAA sequence, instead of the original time series itself.

### 5.1 Implementation Details

The KDE, which is the first step of the discretization process, is critical for guaranteeing the subsequent optimal quantization by means of Lloyd-Max (ref. Alg. 2). In our implementation, the Epanechnikov kernel (20) is employed for minimizing the AMISE criterion, and the smoothness parameter is set according to Silverman's rule in (26).

In order to improve the convergence rate and accuracy of the quantizer, the codewords are initialized by using the  $k$ -means++ algorithm [21], which employs the raw PAA samples for the fast calculation of a good starting point before optimizing upon the estimated density function. This yields an improved performance, in terms of both convergence speed and a lower MSE.

### 5.2 Novel Distance Measures

Notice that the *mindist* and *mindist\_PAA* measures, defined in (2) and (3), respectively, are lower bounds of the true Euclidean distance regardless of the chosen quantization intervals, and hence the lower-bounding property still holds in our proposed representation.

On the other hand, the conventional SAX does not provide arithmetic values for the symbols in the lower-dimensional space, as opposed to the Lloyd-Max quantizer, which is able to do so. As discussed in Sec. 4.2.1, these values are precisely the centroids of the quantization intervals. This feature can be further exploited to define a new distance measure between two symbolic sequences  $Q, C \in \mathcal{C}_A^M$ , as follows,

$$d_s(Q, C) = \sqrt{\frac{N}{M} \sum_{i=1}^M (q_i - c_i)^2}. \quad (40)$$

Although the above distance measure does not lower bound the Euclidean distance, it is the closest to the true one under an MSE criterion. This proximity is up to a distortion caused by (i) the difference between the KDE-based and the true density and (ii) the incapability of Lloyd-Max quantization to minimize globally the MSE. Accordingly, a distance measure between a time series and a symbolic sequence can be derived, which is not possible in the conventional SAX case. Specifically, given  $U \in \mathcal{T}^N$  and  $C \in \mathcal{C}_A^M$ , their distance is defined by

$$d_e(U, C) = \sqrt{\frac{1}{N} \sum_{i=1}^M \left( \sum_{j=(N/M)(i-1)+1}^{(N/M)i} (u_j - c_i)^2 \right)}. \quad (41)$$

In the special case where  $C$  is the symbolic representation of  $U$ , the  $d_e$  is the root mean squared error (RMSE) between  $U$  and its reconstruction from  $C$ .

Note that the proposed method does not need the  $Z$ -normalization pre-processing step. Nevertheless, in order to

ensure that the RMSE has the same scale for all representations, we  $Z$ -normalize all datasets before evaluating the methods.

## 6 DATA-DRIVEN SAX FOR EFFICIENT HIGH-LEVEL TIME SERIES MINING

This section describes a novel SAX representation, hereafter called clustering SAX (cSAX), that provides a descriptive representation for high-level data mining tasks, such as anomaly detection, which is investigated in this work. Although our symbolic representation is designed primarily for data mining tasks that benefit from density-based clustering, it still holds the attractive properties of SAX for database indexing, thus it can be easily integrated in relative systems.

The noticeable difference that makes our proposed symbolic representation effective for anomaly detection lies on the choice of the mean-shift clustering (ref. Alg. 3) for the discretization step. Notice that the alphabet size in our symbolic representation is set automatically by the mean-shift algorithm, thus the only parameter to be defined for the symbolic transformation is the dimensionality  $M$  of the symbolic representation.

### 6.1 Implementation Details

For the mean-shift clustering process we select the Gaussian kernel, instead of the AMISE-optimal Epanechnikov kernel. This choice is motivated by the fact that the Epanechnikov kernel and its derivative are non-continuous at  $\pm\sqrt{5}$ , which is undesirable for mode estimation. The smoothness parameter is set according to (29), whilst the window length  $n$ , which is the only hyper-parameter of our anomaly detection method, is fixed empirically to 50 for all of the datasets.

A problem that arises in practical applications is the need for a training phase of the mean-shift algorithm. The potential lack, or the availability of a very limited amount of historical data from a given data source makes this problem even more complicated. In that case, the clustering method should be able to adapt on-the-fly to the evolving time series stream. To address this problem, a suitable criterion for dynamically re-estimating the clusters from the streaming data is introduced in the next subsection.

### 6.2 Dynamic Mean-Shift Clustering

Having estimated an initial set of clusters, a criterion for dynamically re-estimating the clusters is defined, by utilizing all the data up to the current data point. There are two extreme cases: (i) the clusters are always re-estimated, and (ii) the clusters are never re-estimated. In the first case, the clusters are always up to date, but with a severe delay each time a sample arrives, whilst in the latter case there is no delay, but the estimation is always out of date. None of the above extremes is desirable in practice, thus we propose a computationally tractable process for lying in between the two extremes.

Consider that the current clusters have been estimated using the mean-shift vector in (39) with an arbitrary kernel  $G$ , smoothness parameter  $h_G$ , with  $N$  samples. The mean-shift procedure implicitly estimates the density function by

using another kernel  $K$  that is the shadow of  $G$ . The kernels that are employed by our method are valid probability density functions, that is, they are non-negative and integrate to one. Hence, we can define the standard deviation  $\sigma_K$  of the random variable whose pdf is equal to the kernel  $K$ . The proposed criterion is the following:

**Definition** (Dynamic clustering criterion). The set of clusters are re-estimated when either (i) the most recent window of samples is statistically different from the past windows, or (ii) the most recent sample exceeds the range of previously observed data by a significant degree.

The first case is a statistical deviation criterion. In our anomaly detection method, it is easily determined by the output of the detector itself. That is, the clusters are re-estimated every time an anomaly is detected. The second case is a spatial deviation criterion. A natural scale of spatial deviation is the standard deviation  $\sigma_K$ , which is proportional to the smoothness parameter. For the Gaussian kernel, the standard deviation equals exactly the smoothness parameter, hence it can be defined by (27).

Overall, our proposed dynamic clustering method is based on a hybrid criterion for re-estimating the clusters, with means that are inherent to the density estimation and anomaly detection processes. The anomaly detector tracks the statistical deviation of the data stream, whilst the smoothness parameter of the implicit KDE process is used as a measure of spatial deviation.

## 7 RESULTS

### 7.1 Experimental Evaluation of pSAX

The quality of pSAX is evaluated and compared with its competitors in terms of the TLB (4) and RMSE (41) metrics. The evaluation is done on a selection of datasets, all of which are available in the UCR archive [22]. In what follows, pSAX is compared with the conventional SAX and the adaptive SAX (aSAX) [14] methods. The latter is an alternative data-driven SAX method that employs the  $k$ -means algorithm for the discretization step. For the traditional SAX, which conventionally does not compute numerical values for the symbols, the RMSE (41) is computed by using the centroids of the equiprobable intervals under the Gaussian density function. The pSAX and aSAX are trained on a subset of the available PAA samples of size  $\sqrt{L}$ , where  $L$  is the total number of the PAA samples. Note that to obtain all of the available PAA samples, all subsequences of length  $N$  must be transformed to their PAA representation.

The experimental evaluation is set as follows. We randomly sample two subsequences from the same dataset 1000 times, for each combination of parameters. The subsequences are Z-normalized individually. Both subsequences are used to measure the TLB and one of them is used to measure the RMSE after its dimensionality reduction. The subsequence time series length  $N$  varies in  $\{480, 960, 1440, 1920\}$  and the number of bytes per subsequence varies in  $\{8, 16, 24, 40\}$ . The alphabet size  $\kappa$  varies in  $\{16, 256\}$ , which is 4 and 8 bits per symbol, respectively. Thus, for each length  $N$ , the dimensionality  $M$  of symbolic representation varies in  $\{16, 32, 48, 80\}$  for  $\kappa = 16$  and

in  $\{8, 16, 24, 40\}$  for  $\kappa = 256$ . The results are available in Tables 1-4.

We observe that pSAX outperforms both SAX and aSAX in the vast majority of the experiments, in both TLB and RMSE scores. Also, we notice that the superiority of pSAX is more prominent when i) the number of available bytes is larger and ii) when the alphabet size is smaller. This behaviour is explained by the facts that a) a larger number of bytes provides more PAA samples for pre-training the KDE and Lloyd-Max methods, and b) an adequately large alphabet size drives any discretization method to produce very close discretization intervals. We emphasize that the speedup obtained by indexing with a higher TLB is higher than linear [23]. Thus we expect a greater speedup difference than the difference of TLB in Tables 1-2.

Looking at Tables 1-4, one would infer that the choice of a SAX-based method is a matter of data source and/or parameterization. We assert that it is truly a matter of availability of training data. To this end, we verify this argument by comparing the lengths of the original datasets and the observation we made about the performance of our method versus the available bytes in the symbolic representation.

Interestingly, pSAX and aSAX should asymptotically converge to the same points, as the number of training data grows to infinity. This is because of the relationship between the Lloyd-Max quantizer and the  $k$ -means method (the latter is the finite version of the first), and because of the convergence property of KDE. However, in our experiments we illustrate the efficacy of the methods in the finite regime, and observe the generalization capability of kernel density estimators.

### 7.2 Experimental Evaluation of cSAX

As already mentioned, the quality of cSAX is examined on the task of anomaly detection. To this end, we utilize the detector in Alg. 1. The choice of this detector is based on the idea that, due to its theoretical and algorithmic simplicity, it will highlight the differences among the distinct time series representations. Hereafter, we refer to this detector as the goodness of fit (GoF) detector. The GoF detector depends on two parameters; the alphabet size  $\kappa$  and the window length  $n$ . In our experiments, the window length is set empirically to  $n = 50$ , and is kept fixed for all datasets. Accordingly, the alphabet size is set to  $\kappa = 10$ , except for cSAX that detects automatically the number of clusters.

The anomaly detector is evaluated via i) receiver operating characteristic (ROC) curves and ii) the Numenta Anomaly Benchmark (NAB) [24]. The ROC curves illustrate the efficacy of the detector to discriminate correctly between anomalous and normal samples. On the other hand, NAB provides a large collection of labelled datasets<sup>1</sup> – 47 real-world and 11 synthetic – that are employed in all our experiments. NAB also simplifies the comparison of our detector with other top-tier online anomaly detectors that are already implemented in NAB’s library.

It should be noted that many detectors available in NAB’s library make use of the minimum and maximum values of each dataset. That is also true for the detector we utilize in our experiments, due to the uniform quantization

1. Available: <https://github.com/numenata/NAB/tree/master/data>

TABLE 1  
Tightness of Lower Bound for Alphabet Size  $\kappa = 256$

Dataset	N	Available bytes								
		8			16			24		
		pSAX	aSAX	SAX	pSAX	aSAX	SAX	pSAX	aSAX	SAX
Koski ECG	480	0.560	0.560	0.560	<b>0.699</b>	0.698	0.697	<b>0.781</b>	0.775	0.769
	960	<b>0.385</b>	0.382	<b>0.385</b>	<b>0.573</b>	0.568	<b>0.573</b>	<b>0.652</b>	0.646	<b>0.652</b>
	1440	<b>0.294</b>	0.293	0.293	0.481	0.481	0.481	0.581	0.581	0.581
	1920	0.231	0.231	0.231	0.403	0.403	0.403	0.518	0.518	0.518
Muscle Activation	480	0.613	<b>0.615</b>	<b>0.615</b>	0.710	0.710	0.710	<b>0.771</b>	0.770	0.770
	960	0.776	<b>0.777</b>	<b>0.777</b>	<b>0.837</b>	0.835	0.836	<b>0.865</b>	0.863	0.863
	1440	0.790	0.790	0.790	<b>0.851</b>	0.850	0.850	<b>0.873</b>	0.872	0.872
	1920	<b>0.763</b>	0.762	0.762	<b>0.837</b>	0.835	0.836	<b>0.863</b>	0.862	0.862
Posture	480	0.740	0.740	<b>0.741</b>	<b>0.830</b>	0.827	0.827	<b>0.863</b>	0.858	0.857
	960	0.665	0.665	<b>0.666</b>	<b>0.786</b>	0.782	0.783	<b>0.835</b>	0.830	0.829
	1440	0.616	0.616	<b>0.617</b>	<b>0.751</b>	0.750	<b>0.751</b>	<b>0.811</b>	0.807	0.807
	1920	0.575	0.576	<b>0.577</b>	0.713	0.713	<b>0.714</b>	<b>0.784</b>	0.782	0.782
Respiration	480	0.342	<b>0.344</b>	<b>0.344</b>	0.464	<b>0.466</b>	<b>0.466</b>	0.655	<b>0.656</b>	0.655
	960	0.281	<b>0.283</b>	<b>0.283</b>	0.379	<b>0.381</b>	<b>0.381</b>	0.389	<b>0.392</b>	0.390
	1440	0.257	<b>0.259</b>	<b>0.259</b>	0.336	0.339	<b>0.340</b>	0.399	<b>0.402</b>	0.401
	1920	0.239	0.240	<b>0.241</b>	0.324	<b>0.327</b>	<b>0.327</b>	0.366	<b>0.369</b>	<b>0.369</b>

TABLE 2  
Tightness of Lower Bound for Alphabet Size  $\kappa = 16$

Dataset	N	Available bytes											
		8			16			24			40		
		pSAX	aSAX	SAX	pSAX	aSAX	SAX	pSAX	aSAX	SAX	pSAX	aSAX	SAX
Koski ECG	480	<b>0.641</b>	0.638	0.629	0.774	<b>0.775</b>	0.707	<b>0.835</b>	<b>0.835</b>	0.747	<b>0.883</b>	<b>0.883</b>	0.778
	960	<b>0.531</b>	0.529	0.523	<b>0.656</b>	0.652	0.642	<b>0.727</b>	0.721	0.682	<b>0.819</b>	0.817	0.737
	1440	<b>0.441</b>	0.437	0.433	<b>0.588</b>	0.587	0.581	<b>0.657</b>	0.655	0.645	<b>0.753</b>	<b>0.753</b>	0.698
	1920	<b>0.369</b>	0.367	0.360	<b>0.540</b>	0.539	0.535	<b>0.613</b>	0.611	0.605	<b>0.701</b>	0.697	0.670
Muscle Activation	480	<b>0.637</b>	0.632	<b>0.637</b>	<b>0.744</b>	0.737	0.742	<b>0.798</b>	0.790	0.794	<b>0.848</b>	0.839	0.841
	960	0.756	<b>0.758</b>	0.751	<b>0.799</b>	0.798	0.790	<b>0.823</b>	<b>0.823</b>	0.814	<b>0.852</b>	<b>0.852</b>	0.842
	1440	0.798	<b>0.799</b>	0.783	0.835	<b>0.836</b>	0.821	<b>0.823</b>	<b>0.823</b>	0.814	<b>0.852</b>	<b>0.852</b>	0.842
	1920	0.789	<b>0.791</b>	0.771	0.833	<b>0.834</b>	0.814	0.850	<b>0.851</b>	0.831	<b>0.870</b>	<b>0.870</b>	0.852
Posture	480	<b>0.751</b>	0.744	0.736	<b>0.798</b>	0.787	0.774	<b>0.815</b>	0.807	0.787	<b>0.835</b>	0.825	0.803
	960	<b>0.716</b>	0.710	0.703	<b>0.782</b>	0.781	0.753	<b>0.810</b>	0.805	0.773	<b>0.833</b>	0.830	0.790
	1440	<b>0.685</b>	0.681	0.677	<b>0.768</b>	0.765	0.742	<b>0.801</b>	0.798	0.767	<b>0.830</b>	0.827	0.788
	1920	<b>0.650</b>	0.650	0.647	<b>0.748</b>	0.747	0.728	<b>0.787</b>	0.786	0.757	<b>0.820</b>	0.819	0.781
Respiration	480	<b>0.420</b>	0.417	0.415	<b>0.705</b>	0.695	0.703	<b>0.805</b>	0.801	0.784	<b>0.872</b>	0.869	0.838
	960	<b>0.340</b>	0.335	0.334	<b>0.442</b>	0.441	0.436	<b>0.612</b>	0.605	0.603	<b>0.766</b>	0.765	0.748
	1440	<b>0.300</b>	0.297	0.295	<b>0.359</b>	0.354	0.350	0.458	<b>0.460</b>	0.449	<b>0.658</b>	0.652	0.644
	1920	<b>0.291</b>	0.289	0.285	<b>0.374</b>	0.370	0.362	<b>0.386</b>	0.379	0.373	0.558	<b>0.559</b>	0.545

step. The knowledge of this information violates the principle of online (streaming) algorithms. The only argument in favor of this choice is that the minimum and maximum operating values are often known *a priori*. However, apart from the fact that this is not always true, it is not guaranteed that the datasets' minimum and maximum values coincide with the operating range, and the first provides more significant information than the latter. Our anomaly detector is capable of operating in a really online fashion, thanks to the dynamic mean-shift clustering we described in Sec. 6.2. At the same time, it is capable of pre-training the clustering on historical data, if available.

In the following, we consider the effect of different training set sizes on the detector's performance. Fig. 4 compares the conventional GoF detector, with uniform quantization, and the GoF detector paired with the cSAX, with dynamic mean-shift clustering. For the cSAX we set  $M = N$ , that is, without dimensionality reduction. We emphasize that the training set is used to estimate the clusters for cSAX and the minimum/maximum values for the uniform quantizer, but not the detector's model. In other words, it is a training set for the discretization scheme, not for the detector.

It can be seen that the dynamic mean-shift achieves

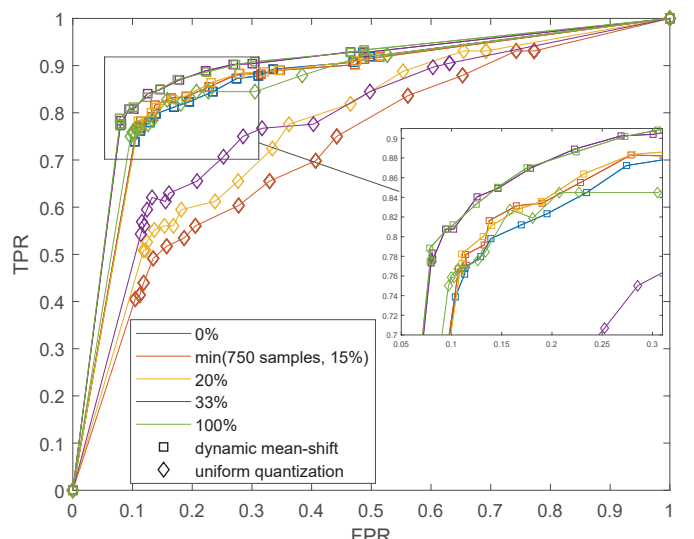


Fig. 4. ROC curves for different training set sizes, with no dimensionality reduction. The training set sizes are expressed in percentages of the original dataset. Note that for the uniform quantizer, the optimal average alphabet size is handpicked ( $\kappa = 10$ , fixed for all datasets), whilst the mean-shift automatically detects the number of clusters.

TABLE 3  
Root Mean Squared Error for Alphabet Size  $\kappa = 256$

		Available bytes											
Dataset	N	8			16			24			40		
		pSAX	aSAX	SAX	pSAX	aSAX	SAX	pSAX	aSAX	SAX	pSAX	aSAX	SAX
Koski ECG	480	0.800	0.800	0.800	0.685	0.685	0.685	<b>0.587</b>	<b>0.587</b>	0.588	<b>0.433</b>	0.434	0.464
	960	0.903	0.903	0.903	0.799	0.799	0.799	0.737	0.737	0.737	0.636	0.636	0.636
	1440	0.944	0.944	0.944	0.859	0.859	0.859	0.796	0.796	0.796	0.717	0.717	0.717
	1920	0.963	0.963	0.963	0.899	0.899	0.899	0.839	0.839	0.839	0.761	0.761	0.761
Muscle Activation	480	0.694	0.694	0.694	0.611	0.611	0.611	0.644	0.644	0.644	<b>0.435</b>	0.436	0.436
	960	0.504	0.504	0.504	0.533	0.533	0.533	0.394	0.394	0.394	<b>0.343</b>	0.344	0.344
	1440	0.484	0.484	0.484	0.406	0.406	0.406	0.372	0.372	0.372	0.331	0.331	0.331
	1920	0.528	0.528	0.528	0.430	0.430	0.430	0.391	0.391	0.391	0.351	0.351	0.351
Posture	480	0.577	0.577	0.577	0.454	0.454	0.454	<b>0.396</b>	0.398	0.398	<b>0.336</b>	0.338	0.342
	960	0.693	0.693	0.693	<b>0.560</b>	0.561	<b>0.560</b>	<b>0.487</b>	0.488	0.488	<b>0.418</b>	0.419	0.420
	1440	0.751	0.751	0.751	0.618	0.618	0.618	<b>0.538</b>	0.539	0.539	<b>0.461</b>	<b>0.461</b>	0.462
	1920	0.785	0.785	0.785	0.663	0.663	0.663	0.584	0.584	0.584	0.499	0.499	0.500
Respiration	480	0.930	0.930	0.930	0.874	<b>0.873</b>	0.874	<b>0.735</b>	0.736	0.736	0.534	0.535	0.537
	960	0.951	0.951	0.951	0.915	0.915	0.915	<b>0.906</b>	<b>0.906</b>	0.907	<b>0.787</b>	<b>0.787</b>	0.791
	1440	0.959	0.959	0.959	0.932	0.932	0.932	0.904	0.904	0.904	<b>0.880</b>	<b>0.880</b>	0.884
	1920	0.964	0.964	0.964	0.937	0.937	0.937	0.919	<b>0.918</b>	<b>0.918</b>	0.890	0.891	0.894

TABLE 4  
Root Mean Squared Error for alphabet size  $\kappa = 16$

		Available bytes											
Dataset	N	8			16			24			40		
		pSAX	aSAX	SAX	pSAX	aSAX	SAX	pSAX	aSAX	SAX	pSAX	aSAX	SAX
Koski ECG	480	<b>0.688</b>	<b>0.688</b>	0.690	<b>0.506</b>	<b>0.506</b>	0.569	<b>0.388</b>	<b>0.388</b>	0.518	<b>0.265</b>	<b>0.265</b>	0.479
	960	<b>0.800</b>	0.801	0.801	<b>0.688</b>	<b>0.688</b>	0.690	<b>0.594</b>	0.595	0.613	<b>0.445</b>	<b>0.445</b>	0.538
	1440	0.863	0.863	0.863	<b>0.757</b>	<b>0.757</b>	0.758	<b>0.687</b>	<b>0.687</b>	0.689	<b>0.565</b>	<b>0.565</b>	0.595
	1920	0.900	0.900	0.900	<b>0.796</b>	0.797	0.797	<b>0.736</b>	<b>0.736</b>	0.738	<b>0.638</b>	<b>0.638</b>	0.644
Muscle Activation	480	<b>0.616</b>	0.617	0.619	<b>0.496</b>	0.498	0.503	<b>0.413</b>	0.417	0.425	<b>0.309</b>	0.313	0.326
	960	<b>0.441</b>	<b>0.441</b>	0.447	<b>0.378</b>	<b>0.378</b>	0.389	<b>0.334</b>	0.335	0.347	<b>0.273</b>	<b>0.273</b>	0.292
	1440	<b>0.409</b>	<b>0.409</b>	0.412	<b>0.355</b>	<b>0.355</b>	0.359	<b>0.322</b>	<b>0.322</b>	0.328	<b>0.273</b>	<b>0.273</b>	0.281
	1920	<b>0.432</b>	<b>0.432</b>	0.435	<b>0.372</b>	<b>0.372</b>	0.376	<b>0.341</b>	<b>0.341</b>	0.345	<b>0.298</b>	<b>0.298</b>	0.304
Posture	480	<b>0.469</b>	0.472	0.480	<b>0.376</b>	0.379	0.410	<b>0.342</b>	0.347	0.378	<b>0.290</b>	0.297	0.342
	960	<b>0.562</b>	0.564	0.570	<b>0.457</b>	0.459	0.478	<b>0.407</b>	0.408	0.436	<b>0.354</b>	0.356	0.396
	1440	<b>0.621</b>	0.622	0.624	<b>0.504</b>	0.505	0.517	<b>0.407</b>	0.408	0.436	<b>0.354</b>	0.356	0.396
	1920	<b>0.667</b>	<b>0.667</b>	0.669	<b>0.541</b>	<b>0.541</b>	0.550	<b>0.478</b>	<b>0.478</b>	0.493	<b>0.414</b>	<b>0.414</b>	0.438
Respiration	480	<b>0.877</b>	0.880	0.878	<b>0.627</b>	0.629	0.635	<b>0.476</b>	0.478	0.493	<b>0.319</b>	0.323	0.356
	960	<b>0.917</b>	<b>0.917</b>	0.918	<b>0.860</b>	0.866	0.866	<b>0.725</b>	<b>0.725</b>	0.738	<b>0.530</b>	0.533	0.559
	1440	0.934	0.934	0.934	<b>0.903</b>	0.905	0.910	<b>0.845</b>	0.851	0.859	<b>0.675</b>	0.677	0.702
	1920	<b>0.938</b>	<b>0.938</b>	0.939	<b>0.898</b>	<b>0.898</b>	0.904	<b>0.886</b>	0.888	0.899	<b>0.768</b>	0.775	0.795

much higher performance for small training set sizes, whilst the performance of the uniform quantizer with 100% training data is practically equal to the performance of the dynamic mean-shift with 0% training data. In advance, it is important that the alphabet size is automatically detected for the dynamic mean-shift method, whilst it required our experimentation to find the best alphabet size for the uniform quantizer. Another important observation is that our dynamic clustering criterion is capable of achieving very close performance between the 0% and 100% training set sizes.

Next, Table 5 includes the NAB scores of our method against the top-performing methods from NAB's library. NAB calculates three different scores by weighing false positives (FPs) and false negatives (FNs) differently: (i) favoring fewer FPs, (ii) favoring fewer FN, and (iii) balancing both FPs and FN. The scores' values vary between 0 and 100 (the higher the better). The methods that require knowledge of the minimum and maximum values are noted with an asterisk. We evaluate cSAX with no pre-training, for a truly online application scenario. Note that the Numenta HTM exploits the minimum and maximum values, but can learn them online, so it is evaluated in a fully online fashion.

TABLE 5  
NAB Scores of the With the cSAX-GoF Detector Without Dimensionality Reduction Against its Competitors

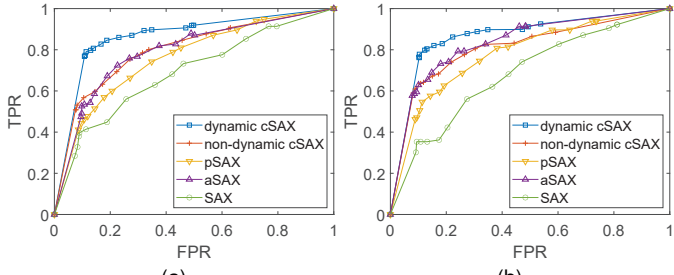
Detector	Standard	Low FP	Low FN
CAD OSE*	69.9	67.0	73.2
GoF*	60.4	50.3	67.6
cSAX-GoF	60.4	49.6	66.0
Numenta HTM	60.0	53.8	63.8
earthgecko Skyline	58.2	46.2	63.9
KNN CAD	58.0	43.4	64.8
Random Cut Forest	51.7	38.4	59.7

\* Require knowledge of the minimum and maximum values of the data.

Notably, the fully online Numenta HTM demonstrates a large decrease in scores, compared to the ones obtained conventionally<sup>2</sup>. Again, we observe that cSAX with no prior information and no need to tune the alphabet size, achieves the same performance as the conventional GoF detector with access to the true minimum and maximum values of the data and having empirically set the best alphabet size.

Our goal at this point is not to achieve the best perfor-

2. Available at: <https://github.com/numenta/NAB#scoreboard>

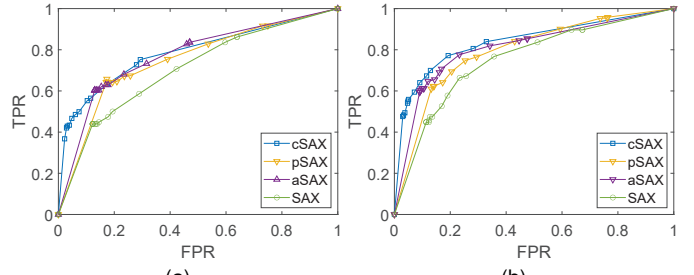


(a)

(b)

(c)

(d)



(a)

(b)

(c)

(d)

Fig. 5. ROC curves of the SAX-based representations (without dimensionality reduction) for different training set sizes: a) 20% of total samples, b) 33% of total samples, c) 66% of total samples, d) 100% of total samples.

mance, but to compare how the underlying representation affects the performance of the same detector, which is the reason we chose a rather simple detector for our experiments. In Fig. 5, we compare the ROC curves for cSAX, pSAX, aSAX and SAX, without dimensionality reduction, for a varying training set size. Notice that the last three require a training set to run. In the case of SAX, the method needs to learn the mean value and the standard deviation of the time series. For all methods except for cSAX, the alphabet size is set to  $\kappa = 10$ . We provide a portion from the beginning of the datasets as a training set and examine the effect of its size. To verify the correctness of our choice of the mean-shift clustering method for high-level analysis, we also evaluate the non-dynamic mean-shift for cSAX when the training set is limited.

We observe that the conventional SAX has the worst performance all the times. The aSAX and the non-dynamic cSAX perform similarly well, both better than pSAX and SAX. But only cSAX is able to detect automatically the alphabet size. More importantly, the superiority of the dynamic cSAX against all the other representations is apparent.

Fig. 6 illustrates the effect of dimensionality reduction on the detector's performance. We hold the training set size to 100% of the total samples and vary the degree of dimensionality reduction  $M/N$  in  $\{1/32, 1/16, 1/8, 1/4\}$  (from large to low degree of dimensionality reduction). As it can be seen, the conventional SAX has the worst performances, whereas cSAX clearly outperforms all the other SAX-based representations.

## 8 CONCLUSIONS AND FUTURE WORK

This paper proposes two novel non-parametric, data-driven symbolic representations, named pSAX and cSAX, by modifying the discretization process of the traditional SAX

Fig. 6. ROC curves of the SAX-based representations on 100% training set for different degrees of dimensionality reduction: a)  $M/N = 1/32$ , b)  $M/N = 1/16$ , c)  $M/N = 1/8$ , d)  $M/N = 1/4$ .

method. The proposed methods achieve to negate two restrictive assumptions of the traditional SAX, namely, the Gaussian distribution and the equiprobability of the symbols. The derived representations are based on kernel techniques to precisely adapt to the underlying data statistics. Furthermore, the pSAX representation employs the Lloyd-Max quantizer for general data compaction, whilst cSAX employs the mean-shift clustering for high-level time series analysis. A dynamic clustering mechanism is also introduced, such that the cSAX-based representation performs in a fully online fashion, enhancing its quality and simplifying its application for online data mining tasks. Equally importantly, both the pSAX and cSAX preserve the lower-bounding property and are shown to outperform the conventional SAX, as well as the aSAX, an alternative data-driven SAX-based representation. In addition, we propose two novel distance measures, which are not lower-bounding, but are optimal in the sense of mean squared error. Finally, we verify theoretically – and propose a solution thereupon – a previously observed phenomenon that reduces the variance at the intermediate piecewise aggregate approximation, causing an additional information loss when left unnoticed.

The experimental evaluation of the methods is performed on a large collection of heterogeneous datasets. The experiments showed that pSAX produces symbolic representations that are most often of higher quality than its competitors, whereas the superiority is more apparent in the settings of small alphabet size. The proposed cSAX is evaluated on the task of anomaly detection, both with and without dimensionality reduction. It is shown that the dynamic criterion is able to boost the performance of the anomaly detector, such that very good performance is achieved even when the clusters are not pre-trained. At the same time, both the non-dynamic and the dynamic mean-

shift outperforms the alternative SAX-based representations for the purpose of anomaly detection. Very importantly, cSAX eliminates the need to tune the symbolic alphabet size, as it is automatically detected.

Currently, the pSAX method has not been tested in computationally demanding indexing scenarios. The paradigm of iSAX [23] shows that scalable indexing is possible when the discretization scheme is hierarchical. Motivated by this, we are interested in extending the Lloyd-Max quantizer in a hierarchical framework. Early experimentation shows that this is possible with virtually no decrease in the tightness of lower bound (TLB). At the same time, the proposed cSAX has not been evaluated in terms of TLB. It is of interest to see how the dynamic mean-shift affects the TLB, due to the varying quantization intervals. An extension of both pSAX and cSAX can be considered for the case of multi-channel time series, where the different channels are correlated. In that case, optimal discretization can be achieved by multivariate kernel density estimators for cSAX and vector quantizers for pSAX.

## APPENDIX

### PROOF OF THEOREM 3.1

*Proof.* Denote with  $G(x_i)$  the pmf of the quantized  $X$  under the wrong distribution  $g(x)$ . Assuming optimal coding under  $G(x_i)$ , the expected description length is given by (ref. [18, Thm. 5.4.1])

$$\begin{aligned}
 \mathbb{E}[l(X^\Delta)] &= \sum_{x_i} P(x_i) \lceil \log \frac{1}{G(x_i)} \rceil \\
 &< \sum_{x_i} P(x_i) \left( \log \frac{1}{G(x_i)} + 1 \right) \\
 &= \sum_{x_i} P(x_i) \left( \log \frac{P(x_i)}{G(x_i)} \frac{1}{P(x_i)} + 1 \right) \\
 &= \sum_{x_i} P(x_i) \log \frac{P(x_i)}{G(x_i)} + \sum_{x_i} P(x_i) \left( \log \frac{1}{P(x_i)} + 1 \right) \\
 &= \sum_{x_i} f(x_i) \Delta \log \frac{f(x_i) \Delta}{g(x_i) \Delta} + \sum_{x_i} f(x_i) \Delta \left( \log \frac{1}{f(x_i) \Delta} + 1 \right) \\
 &= \sum_{x_i} f(x_i) \Delta \log \frac{f(x_i)}{g(x_i)} - \sum_{x_i} f(x_i) \Delta (\log(f(x_i) \Delta) - 1) \\
 &= \sum_{x_i} f(x_i) \Delta \log \frac{f(x_i)}{g(x_i)} - \sum_{x_i} f(x_i) \Delta \log f(x_i) \\
 &\quad - \sum_{x_i} f(x_i) \Delta (\log \Delta - 1) \rightarrow D(f \parallel g) + h(X) + \log \frac{1}{\Delta} + 1, \\
 &\text{as } \Delta \rightarrow 0,
 \end{aligned} \tag{42}$$

where Riemann integrability is assumed in the last line of (42).

Similarly, it can be shown that

$$\mathbb{E}[l(X^\Delta)] \geq D(f \parallel g) + h(X) + \log \frac{1}{\Delta}, \quad \text{as } \Delta \rightarrow 0. \tag{43}$$

□

## REFERENCES

- [1] C. Faloutsos, M. Ranganathan, and Y. Manolopoulos, "Fast subsequence matching in time-series databases," in *Proc 1994 ACM SIGMOD Int. Conf. Manage. Data*, ser. SIGMOD '94. New York, NY, USA: ACM, 1994, p. 419–429.
- [2] J. Lin, E. Keogh, S. Lonardi, and B. Chiu, "A symbolic representation of time series, with implications for streaming algorithms," in *Proc. 8th ACM SIGMOD Workshop Res. Issues Data Mining Knowl. Discovery*, ser. DMKD '03. New York, NY, USA: ACM, 2003, p. 2–11.
- [3] P. Ordonez, T. Armstrong, T. Oates, and J. Fackler, "Using modified multivariate bag-of-words models to classify physiological data," in *2011 IEEE 11th Int. Conf. Data Min. Workshops*, 2011, pp. 534–539.
- [4] B. Chiu, E. Keogh, and S. Lonardi, "Probabilistic discovery of time series motifs," in *Proc. 9th ACM SIGKDD Int. Conf. Knowl. Discovery Data Mining*, ser. KDD '03. New York, NY, USA: ACM, 2003, p. 493–498.
- [5] I. P. Androulakis, J. Vitolo, and C. Roth, "Selecting maximally informative genes to enable temporal expression profiling analysis," in *Proc. Found. Syst. Biol. Eng.*, 2005.
- [6] Y. Wang, Q. Chen, C. Kang, and Q. Xia, "Clustering of electricity consumption behavior dynamics toward big data applications," *IEEE Trans. Smart Grid*, vol. 7, pp. 2437–2447, 09 2016.
- [7] C. Miller, Z. Nagy, and A. Schlueter, "Automated daily pattern filtering of measured building performance data," *Automation in Construction*, vol. 49, pp. 1 – 17, 2015.
- [8] S. Aghabozorgi and Y. W. Teh, "Stock market co-movement assessment using a three-phase clustering method," *Expert Syst. with Appl.*, vol. 41, no. 4, Part 1, pp. 1301 – 1314, 2014.
- [9] E. Parzen, "On estimation of a probability density function and mode," *Ann. Math. Statist.*, vol. 33, no. 3, pp. 1065–1076, 09 1962.
- [10] S. P. Lloyd, "Least squares quantization in PCM," *IEEE Trans. Inf. Theory*, vol. 28, pp. 129–136, 1982.
- [11] J. Max, "Quantizing for minimum distortion," *IRE Trans. Inf. Theory*, vol. 6, no. 1, pp. 7–12, 1960.
- [12] Yizong Cheng, "Mean shift, mode seeking, and clustering," *IEEE Trans. Pattern Anal. Mach. Intell.*, vol. 17, no. 8, pp. 790–799, 1995.
- [13] D. Comaniciu and P. Meer, "Mean shift: a robust approach toward feature space analysis," *IEEE Trans. Pattern Anal. Mach. Intell.*, vol. 24, no. 5, pp. 603–619, 2002.
- [14] N. D. Pham, Q. L. Le, and T. K. Dang, "Two novel adaptive symbolic representations for similarity search in time series databases," in *2010 12th Int. Asia-Pacific Web Conf.*, 2010, pp. 181–187.
- [15] M. Butler and D. Kazakov, "SAX discretization does not guarantee equiprobable symbols," *IEEE Trans. Knowl. Data Eng.*, vol. 27, no. 4, pp. 1162–1166, 2015.
- [16] Q. Wang and V. Megalooikonomou, "A dimensionality reduction technique for efficient time series similarity analysis," *Inf. Syst.*, vol. 33, no. 1, pp. 115–132, 2008.
- [17] C. Wang, K. Viswanathan, L. Choudur, V. Talwar, W. Satterfield, and K. Schwan, "Statistical techniques for online anomaly detection in data centers," in *12th IFIP/IEEE Int. Symp. Integr. Netw. Manage. (IM 2011) Workshops*, 2011, pp. 385–392.
- [18] T. M. Cover and J. A. Thomas, *Elements of Information Theory* (Wiley Series in Telecommunications and Signal Processing). USA: Wiley-Interscience, 2006.
- [19] V. A. Epanechnikov, "Non-parametric estimation of a multivariate probability density," *Theory of Probability & Its Applications*, vol. 14, no. 1, pp. 153–158, 1969.
- [20] B. W. Silverman, *Density Estimation for Statistics and Data Analysis*. London: Chapman & Hall, 1986.
- [21] D. Arthur and S. Vassilvitskii, "k-means++: the advantages of careful seeding," in *SODA '07: Proc. eighteenth annu. ACM-SIAM symp. Discrete algorithms*. Soc. Ind. Appl. Math., 2007, pp. 1027–1035.
- [22] H. A. Dau *et al.*, "The UCR time series classification archive," October 2018, [https://www.cs.ucr.edu/~eamonn/time\\_series\\_data\\_2018/](https://www.cs.ucr.edu/~eamonn/time_series_data_2018/).
- [23] J. Shieh and E. Keogh, "iSAX: Indexing and mining terabyte sized time series," in *Proc. 14th ACM SIGKDD Int. Conf. Knowl. Discovery Data Mining*, ser. KDD '08. New York, NY, USA: ACM, 2008, p. 623–631.
- [24] A. Lavin and S. Ahmad, "Evaluating real-time anomaly detection algorithms – the numenta anomaly benchmark," in *2015 IEEE 14th Int. Conf. Mach. Learn. Appl. (ICMLA)*, 2015, pp. 38–44.